Human Extracellular Matrix (ECM)-like Collagen and its Bioactivity

Hui Zhou[1], Wenwei Li[2], Lixin Pan[2], Tianci Zhu[2], Teng Zhou[2], E Xiao[2*] and Qiang Wei[1,2*]

1. State Key Laboratory of Polymer Materials and Engineering, College of Polymer Science and Engineering, Sichuan University, Chengdu 610065, China

2. Hunan Maybio Bio-Pharmaceutical Co., Ltd., Changsha 410000, China

*Address correspondence to:wei@scu.edu.cn(Q.W.); xiaoe1986@vip.163.com(E.X.)

Keywords: Extracellular matrix, native-like collagen, cell-derived matrix, hierarchical structure

ABSTRACT

Collagen, the most abundant structural protein in the human extracellular matrix (ECM), provides essential support for tissues and guides tissue development. Despite its widespread use in tissue engineering, there remains uncertainty regarding the optimal selection of collagen sources. Animal-derived sources pose challenges such as immunogenicity, while the recombinant system is hindered by diminished bioactivity. In this study, we hypothesized that human ECM-like collagen (hCol) could offer an alternative for tissue engineering. In this study, a facile platform was provided for generating hCol derived from mesenchymal stem cells (MSCs) with a hierarchical structure and biochemical properties resembling native collagen. Our results further demonstrated that hCol could facilitate basal biological behaviors of

human adipose-derived stem cells (hASCs), including viability, proliferation, migration and adipocyte-like phenotype. Additionally, it could promote cutaneous wound closure. Due its high similarity to native collagen and good bioactivity, hCol holds promise as a prospective candidate for i*n vitro* and *in vivo* applications in tissue engineering.

1. Introduction

Collagen is the most abundant structural protein of connective tissues including skin, tendon and cartilage in mammals. As a major component of the extracellular matrix (ECM), collagen serves many functions, including regulation of cell adhesion, support for cell migration and guidance of tissue development [1, 2]. Due to its superior biocompatibility and low immunogenicity, collagen has proven safe and effective in a various clinical applications, such as wound healing, skin regeneration and etc [3-5]. It acts not only as reliable replacement of damaged tissues, but also regulates cell's biological behaviors and phenotype i*n vitro* [6]. The ever-increasing demand for collagen has has necessitated the exploration of native or native-like collagen. At present, collagen can be extracted from animal sources such as cows, pigs, bovine or marine life, but the issue of transmissible diseases or lower thermal stability limits the use of collagen from these sources [7, 8]. Additionally, the recombinant collagen can serve as an alternative source to animal collagen; however, it has low structural stability and bioactivity due to a lack of proper post-translational modifications [9, 10]. The production of correctly post-translationally modified recombinant human collagen is very complicated, as the native collagen production requires collagen-specific chaperones, foldases and post-translational modification enzymes [11]. These limitations of native collagen pose obstacles to the widespread application of collagen-based engineered scaffolds *in vitro* and *in vivo.*

Recently, ECM derived from cultured mammalian cells is gaining momentum due to the successful demonstration of glycosylation and key post-translational

modifications, which closely mimics the composition and organization of natural collagen [12, 13]. Specifically, the biosynthesis of nature collagen *in vivo*, involving numerous intracellular and extracellular steps, causes it to have a multi-hierarchical fibrous architecture [14]. Similar to biosynthesis *in vivo*, collagen derived by cells can be folded into a triple helix with proper modification and adequate cell ligands to collagen-specific receptor (e.g., $\alpha_1\beta_1$, $\alpha_2\beta_1$, $\alpha_3\beta_1$, etc.), which can modulate diverse cell functions [15-17]. Besides, collagen derived by cells in the extraceullular environment can be further assembled into supramolecular collagen aggregates recognized by an axial periodicity, known as D-period [18]. These advanced structures (triple helix and D-period feature) can be essential for many biological process or relevant pathological conditions, as they can impact collagen mechanical properties and cell-collagen crosstalk [19, 20]. Although collagen derived by cells have these advantages theoretically, it is important to validate its multi-level structure and its bioactivity.

In contrast to other sources, collagen derived by cells can be customized by selecting the type(s) of cells used to generate the ECM, the culture system (e.g. 2D versus 3D culture), the application of external stimuli to modulate ECM production and etc. Taking advantages of this, there are several methods to generate such matrix proteins like 2D culture systems with protein coating and 3D culture systems (e.g., porous materials [21], microcarrier templating [22] and hydrogel network) [23]. To increase collagen production, we used porous materials with interconnected pores, which are ideal scaffolds for the colonization of seeded cells and matrix accumulation

due to large specific surface areas and free space [24, 25]. Polyethersulfone (PES) scaffold was chosen due to its optimal hydrophilicity that benefits protein absorption and further cell attachment. Briefly, the porous PES scaffold was cultured with human mesenchymal stem cells (hMSCs), resulting in the production of matrices composed mainly of types I and III collagen, proteoglycans and glycoproteins. Followed by purification and lyophilization, human ECM-like collagen (hCol) was generated from this collagen-rich ECM containing mainly type I and type III collagen. To validate if native-like property and hierarchical structures formed in hCol, biochemical and structural characterization of hCol were performed as compared to native animal collagen, including molecular weight, glycosylation, disulfide linkage and protein secondary structure, triple helix and fibril structure. Furthermore, to confirm the bioactivity of hCol, the influences of hCol on stem cell proliferation, migration and differentiation were studied. The novelty of this work is to confirm native-like structures in cell-derived collagen and it is the first time that MSC-derived collagen has been applied *in vitro* and *in vivo.*

2. Materials and Methods

2.1 Preparation of hCol derived from hMSCs

For synthesis of cell scaffold, PES was used as a cell culture platform because of its proper hydrophobicity to enhance protein adhesion for cell growth. Briefly, an 8 wt % PES solution was extruded into a water bath by liquid-liquid phase separation and dissolved in N, N-Dimethylacetamide (DMAC) under ultrasound for 15 seconds.

Water was then added to terminate the dissolution, resulting in synthesis of PES scaffolds. Subsequently, the scaffolds were thoroughly washed in boiling water to remove the solvent, followed by steam, alcohol and UV sterilization before cell culture. hMSCs were then seeded at a density of $1x10^5/cm^2$ in the scaffolds with a customized medium [26]. After a 14-day culture, the scaffolds were deceullarized and purified to collect collagen-rich ECM following a protocol that was similar to that previously described [8, 27]. Briefly, the scaffolds were treated with a precooled 0.25% trypsin-EDTA solution for 20 minutes, followed by another 20-minute treatment with the addition of 3% Triton X-100. Afterwards, the scaffolds were washed with deionized water and freeze-dried. To remove PES materials, the scaffolds were dissolved in DMSO followed by a 10-minute centrifugation step at 8000 rpm. The ECM was then collected by washing the precipitate with DMSO and deionized water, respectively, 3 times each. Subsequently, the ECM was treated with 0.5M acetic acid for 24h at 4˚C, then centrifuged and pepsin (1 mg/mg protein) was added overnight. Afterwards, the supernatant was salted-out with NaCl for 12h and dialysed against 0.1 M acetic acid with a molecular weight of 7 kDa before being lyophilised and stored at -20 °C until further use.

To monitor *in vitro* expansion of stem cells, hMSC cell line was transfected with retroviral vectors (GeneChem, NM_009354) containing human telomerase reverse transcriptase (hTERT) gene according to the manufacturers protocol. The immunofluorescence fluorescence of transduced cells (hTERT-hMSCs) using rabbit anti-TERT antibodies (Abcam, Ab191523) was captured under fluorescence

microscopy (Leica DMi8, Leica Microsystems). The hTERT-hMSCs were cultured in standard Dulbecco's modified eagle's medium (DMEM; Gibco, 21885-025) supplemented with 10% fetal bovine serum (FBS; Gibco, 10099141C) and 1% penicillin/streptomycin (PS; Gibco, 15140122) at 37 °C with 5% CO_2.

2.2 Biochemical Characterization of hCol

2.2.1 SDS-PAGE

Lyophilized samples of bovine type I collagen (bCol I) and hCol were dissolved at a concentration of 0.2 mg/mL in 3% acetic acid at 4˚C for 24 h. The dissolved samples were mixed at a 4:1 ratio (v/v) with the sample buffer (0.5 M Tris-HCl, pH=6.8, containing 20% SDS (10% w/v), 10% beta-mercaptoethanol, 0.5% bromophenol blue and 20% glycerol) and boiled for 5 minutes. Then the protein samples (20 μg/well) were loaded on 12.0% polyacrylamide gel including a 4% stacking gel, subjected to electrophoresis at a constant voltage of 80 V for 15 minutes and then at 120V for 15 minutes. The gels were further stained with Goomassie G-250 to captuer images.

2.2.2 Mass spectrometry (LC-MS/MS)

The lyophilized samples (hCol and bCol I) were digested with enzymes (Promega), including trypsin, chymotrypsin & Glu-C, chymotrypsin, trypsin & Glu-C and elastase for glycan analysis, while the samples were digested with trypsin and Glu-C for disulfide bond analysis. Then, the digested protein (0.2 μg each) were analyzed on an Easy-nLC 1200 with a nanospray source connected to a Q Exactive Hybrid Quadrupole-Orbitrap mass spectrometer (Thermo Fisher Scientific, Waltham, MA). The top 10 most abundant precursor ions were selected from a 300 m/z to

1800 m/z full scan for collisional activation dissociation (HCD). The raw files were analyzed and searched against the target protein database based on the species of the samples using PLINK software version 2.3.5 (Christopher Chang/Grail Inc) [28]. The maximum missed cleavages were set to 3; the precursor ion mass tolerance was set to 20 ppm, and the tolerance was set to 0.02 Da.

2.3 Structural Characterization of hCol

2.3.1 FTIR

The lyophilized bCol I and hCol were examined by Fourier transform infrared spectrometry (FTIR, Nicolet 560, America). Both the background and samples were both scanned with 32 accumulations in the wavenumber range of 4000 to 500 cm^{-1}. The spectra were processed using automatic baseline calibration and 11-point Savitzky-Golay smoothing with order of 3 for further analysis.

2.3.2 Raman spectroscopy

Raman spectroscopy was performed on the sample in a labRam HR evolution microscope (HORIBA France SAS,Palaiseau, France) with a 532 nm continuous wave solid-state laser and a 50X air lens (N.A.=0.5). The spectra were collected from 600 to 1800 cm^{-1} with 12 accumulations and acquisition time of 10 seconds each. The raw spectra were processed by subtracting background fluorescence using a 5th-order polynomial fit and smoothed by Savitzky-Golay filters with an order of 3 and a window size of 11 in Labspec 6.0 software (Horiba, France) as previously described [29]. The spectra were then processed with standard normal variate normalization in Matlab®. The processed amide I band in the range of 1600-1700 cm^{-1} was

decomposed in multiple sub-bands based on Levenberg-Marquardt algorithm in OriginPro 2021 (OriginLab Corporation, Northampton, MA, USA). All the secondary structural content was estimated by dividing the areas under each sub-band by the whole area of amide I band and reported as a percentage.

2.3.4 Circular Dichorism (CD) spectroscopy

CD spectra of hCol and bCol I (0.25 mg/ml in pH 12 NaOH) were obtained using Chirascan V100 Spectrometer (Applied Photophysics Ltd, UK) using 0.5 mm quartz cuvettes. The spectrum (190-260 nm) for the NaOH solution (pH 12) was subtracted from each sample spectrum and then smoothed using Savitsky-Golay with a polynomial order of 2 and a window size of 3.The molar ellipticity [Θ] was calculated by the following equation:

$$[\Theta] = (\Theta \times 100 \times M_w)/(C \times l) \quad (1)$$

where Θ was ellipticity obtained from CD spectrometer, M*w* is the molecular weight of amino acid residue, C is the concentration of sample, and *l* is the width of cuvette. The thermal curves of triple helix were monitored by the molar ellipticity at 222nm with increasing the temperature from 22˚C to 55˚C at a rate of 1˚C/min.

2.3.5 Electron microscopy

The scanning electron microscopy (SEM) was performed using an Apreo S HiVoc (Thermo Fisher Scientific, FEI) operated at 5 kV. All SEM samples were observed with gold coating with a layer of about 5 nm. Droplets (10 μL, 0.004 mg/mL) of the protein solution in NaoH (pH 9) are placed on ultrathin carbon film on copper grids (Ted Pella, Inc. USA). The transmission electron microscopy (TEM),

aberration-corrected high-angle annular dark-field scanning TEM (AC HAADF-STEM) and energy dispersive spectroscopy (EDS) mapping were achieved on Bruker Nano GmbH Quantax (ThermoFisher Scientific, USA) using an electron acceleration energy of 200 kV with a cold field emission electron source.

2.4 The effect of hCol on cell behaviors and phenotype

2.4.1 Cell proliferation

To study the effect of hCol on cell proliferation, the cell viability of hASCs was measured using CCK-8. The hASCs were planted into 96-well plates (2000 cells per well) and CCK-8 solution (10 μL/well) was added to measure cell viability. The optical density (OD) at 450 nm wavelength was measured using the Multiskan FC (Thermo Fisher Scientific, Inc, Waltham, MA). The cell growth was quantified by counting number of cells per mL in cell suspension using a hemocytometer at different hours after cell seeding and bright filed images were taken before counting.

2.4.2 Cell migration

A scratch test was used to determine the effect of hCol on the migration ability of human adipose stem cells (hASCs). Briefly, hASCs were cultured on 6-well plates (5×10^4/mL per well) until reaching 90% confluence using complete growth medium (10% FBS/1%PS/DMEM) and then washed with PBS. Cell scratches were made with a 200-μL pipette tip and the bright field images were taken at 0, 24, and 48 h after the scratch. For comparison of the effect of different collagen groups on cell migration, hASCs were cultured respectively in medium supplemented with 10 μg/mL hCol, medium with 10 μg/mL bCol I and complete growth medium alone (blank control).

The migration rate was calculated using wound area closure equation previously described.[30] To explore if structure of hCol plays a role in cell migration, hCol was exposed to the following processes and then used in cell migration in the same way: alkaline, steam sterilization, vapor hydrogen peroxide (VHP) and radiation treatment, respectively. For alkali treatment, hCol was treated with a solution of 3.0% NaOH (w/v), 1.9% monomethylamine (v/v) at 20˚C. For steam sterilization, hCol was autoclaved at 140 kN/m^2 steam pressure at 126°C for 11 minutes. For VHP, hCol was kept in a peroxide solution at room temperature for 30 minutes. For radiation, hCol was exposed to a radioactive cobalt-60 source at ambient temperature until a minimum dose of 25 kGy was achieved.

2.4.3 Cell differentiation

To differentiate cells, hASCs were seeded at a density of 1×10^5 per well in a 6-well plate with adipogenic induction medium (AIM) that contains 1μM dexamethasone, 0.5mM 3-isobutyl-methylxanthine, 10 μg/mL insulin and 0.2mM indomethacin (Sigma-Aldrich, St. Louis, MO). For blank control, hASCs were cultured in complete growth medium (DMEM/10%FBS/1%PS). To study the effect of hCol on cell differentiation, hASCs were cultured on a 6-well plate coated with 1mg/mL hCol in AIM medium and compared with those in AIM medium and complete growth medium alone, respectively. After 14-day culturing, total RNA were extracted to analyze differentiation markers, including peroxisome proliferator-activated receptor (PPAR2γ) and key enzyme gene lipoprotein lipase (LPL). After 21 days of differentiation, cells were fixed with 75% ethanol and stained with Oli Red O solution

(Cyagen Biosciences Inc., OILR-10001) for 30 minutes. Bright-field images were acquired on a Leica DMi8 Microscope. For gene expression, each RNA sample (1 μg) was used to synthesize cDNA with a PrimeScript® RT Reagent Kit (Takara, Japan) following the manufacture's recommendations. The PPARγ2 gene was amplified and quantified using the forward primer 5′-GGG TGA AAC TCT GGG AGA TTC TC-3′; reverse primer 5′-GAT GCC ATT CTG GCC CAC-3′ and the LPL gene was amplified and quantified using forward primer 5′-ATTCTCCCTCCGCAAACCC-3′ and reverse primer 5′-GGAGGTGCTGTTGAAGGTG-s′). At reverse transcription reaction, cDNA (SYBR Green I, Invitrogen, Carlsbad, CA, USA) was used as the template for real-time quantitative PCR for LPL and PPARγ2 while glyceraldehyde-3-phosphate dehydrogenase (GAPDH) was utilized as a internal control. The typical cycling conditions consisted of an initial denaturation step at 94 ˚C for 4 minutes, 35 cycles of amplification at 94 ˚C for 20 s, 60 ˚C for 30 s and 72 ˚C for 30 s. The relative expression of gene was measured as the relative expression of mRNA in the indicated groups to control (normalized to the corresponding GAPDH values).

2.5 The effect of hCol on wound closure in mouse tail skin

All procedures involving the use of animals in this study were prospectively reviewed and approved by the Institutional Animal Care and Use Committee. This study was conducted in adherence to the guidelines was approved by the ethical committee (No. 2021911 A) of West China Hospital, Sichuan University. During the experiment, the animals had free access to water and food. Here, five six- to eight-week-old male SPF

BALB/c mice with body weight of 18-20 g were used for this study. The full-thickness wounds corresponding to the template area (10 × 5mm) were created to the dorsal surface of the mice tail by sterile gauge scalpels (Becton Dickinson Co., Hancock, NY). For experimental group, hCol (10 μg/mL) was applied to the wounded areas twice daily while the commercial recombinant collagen (10 μg/mL, Shanxi Jinbo Bio-pharmaceutical) was applied as control in the same way. Photographs of the wounds from a fixed distance at regular time intervals were taken. After inducing anesthesia with an excessive dose of isoflurane, the mice were euthanized through cervical dislocation. The wound sites after day 14 were paraffin-sectioned, hematoxylin and eosin (H&E) staining was performed and the images were acquired on a Leica DMi8.

2.5 Statistical analysis

Statistical analyses were performed using the software JMP Pro 12 (SAS company, Car, NC, USA). An unequal variance t-test (two-sample t-test) would be used for comparing proliferation as well as adipogenesis (between AIM group and AIM+hCol group). A pooled two-sample student t-test was used for comparing wound closure area. And post-hoc Dunnett's test was used to determine significance of hTERT intensity among different culturing day compared to control, cell migration treatments compared to control (no treatment) as well as gene expression among different medium as compared to control medium. $P \leq 0.05$ was considered statistically significant.

3. Results and Discussion

3.1 Preparation of human ECM-like collagen

To confirm if the PES culture platform is suitable for producing cell derived matrix, the growth of hTERT-hMSCs was monitored. As shown in Fig. 1a and 1b, the continuous increase of TERT expression with culturing days indicated the well growth of hMSC and ensures a critical mass of hMSCs without influence of transcription. The SEM images showed pores in PES scaffolds, each about a few hundred micrometer wide, where hMSCs can grow (Fig. 1c). After ten days of cell seeding, cells were well spread over the surface and cross section of porous PES scaffold with cell membrane extensions (filopodia and lamellipodia). Cells merged completely and intercellular connections were barely visible, suggesting that PES scaffolds had good biocompatibility for hMSC attachment. The decellularization before collecting ECM got rid of cellular components (Fig. 1d) and the PES template was further removed (Fig. 1e and 1f) without minimal damage of the scaffold structure.

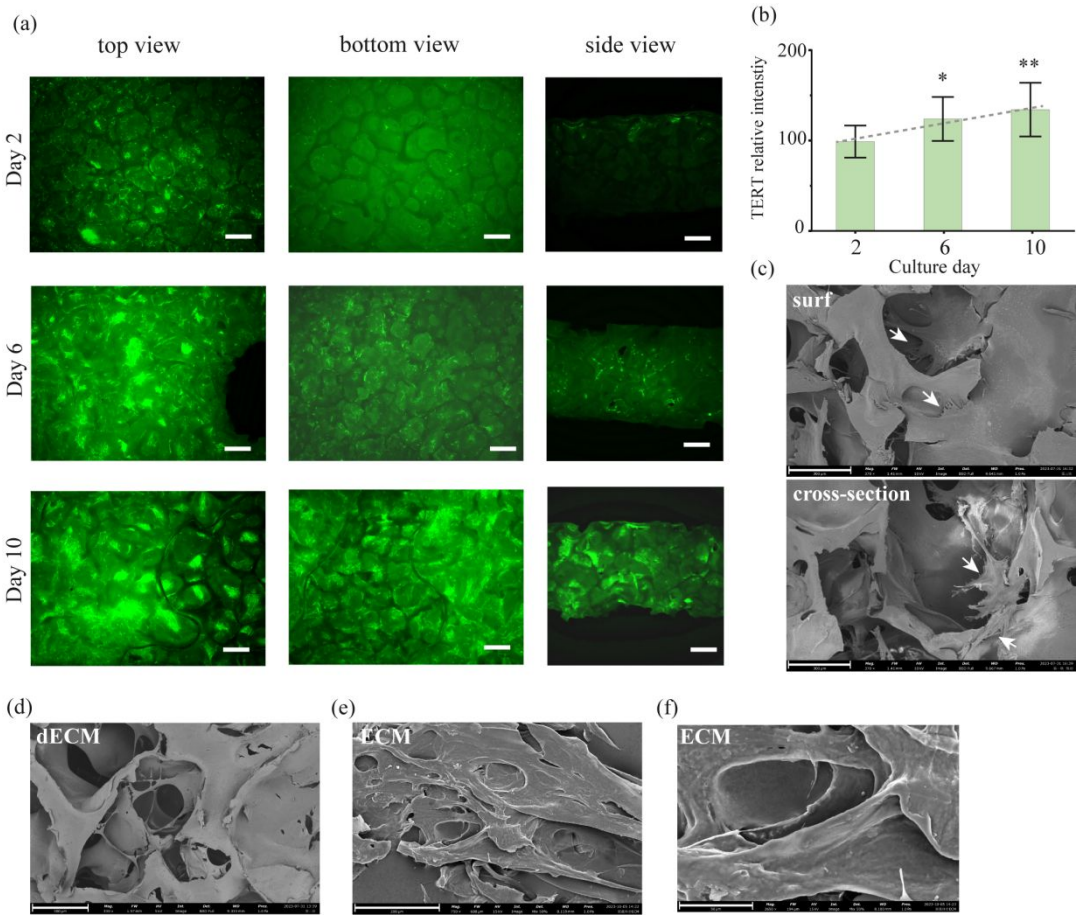

Figure 1. hTERT-hMSC growth and morphology of PES scaffold and ECM. (a) Representative confocal 3D scanning images of the apical surface (top view), the basal surface (bottom view) and side view of PES scaffold subjected to staining for hTERT (green) after culturing for 2, 6 and 10 days, scale bar= 500 μ m. Statistical difference: *p < 0.05 and **p < 0.01 compared with the day 2 (control) when cells start to express hTERT. (b) The relative TERT fluorescent intensity change in PES scaffolds with different culturing days. Data shown are the means ± SD for 3 independent experiments. SEM images of (c) the surface and the cross-section of PES scaffold (day 10), (d) the scaffold surface after decellularization (day 14), (e) ECM after removing PES materials and (f) ECM at higher magnification. The scale bars, 300 μm (1c and 1d), 200 μm (1e) and 100 μm (1f).

3.2 Biochemical characterization of human ECM-like collagen (hCol)

The collected ECM was purified and lyophilized to obtain massive hCol as seen in Fig. 2a. The mass proteomics analysis demonstrated that the relative staining intensity of α1 band was higher than that of α2 band in both groups. Considering the native type I collagen mostly occurs as a heterotrimer with two identical α1-chains and one

α2-chain [31], the mass analysis implied that hCol was mainly composed of type I collagen (Fig. 2b and 2c). This was in agreement with SDS-PAGE data, where the percentage of α1-chain is about 1.8 times of α2-chain as seen in Fig. 2d. The electrophoretic protein pattern showed hCol was composed of α1 chains (132 kDa) and α2 chains (122 kDa), which was similar to native bovine collagen (bCol I) consisting of α1(132 kDa) and α2 chains (123 kDa), as seen in Fig 2d. Furthermore, the quantitative glycoproteomic data were then analyzed to investigate whether hCol showed distinct glycopeptide features as compared with bCol I. As shown in Fig. 2e, collagen chains were glycosylated at Ser_3, Ser_{1141} and Thr_{1327} sites in both bCol and hCol, though the glycosylation at Ser_{1267} were present in hCol while absent in bCol I. Among all O-glycan sites, the modification at Ser_{1141} appears to be most abundant for both bCol I and hCol. For N-glycosites, N1267 and N1365 were observed to be modified and N1365 is predeominantly present in both groups (Fig. 2f). These observations collectively indicated a very similar pattern of glycosylation on collagen chains for both groups. However, N-glycan structures between bCol I and hCol were different to some degree. All N-glycans between two shared a common core structure including the first two N-Acetylhexosamine (HexNAc) residues and the first three hexose (Hex) residues. Nevertheless, N-glycans of hCol exist as high-mannose type consisting of only HexNAc and Hex residues, while N-glycans of bCol I exist as complex type with additional sugars such as fucose (Fuc) and sialic acid (NeuNAc).

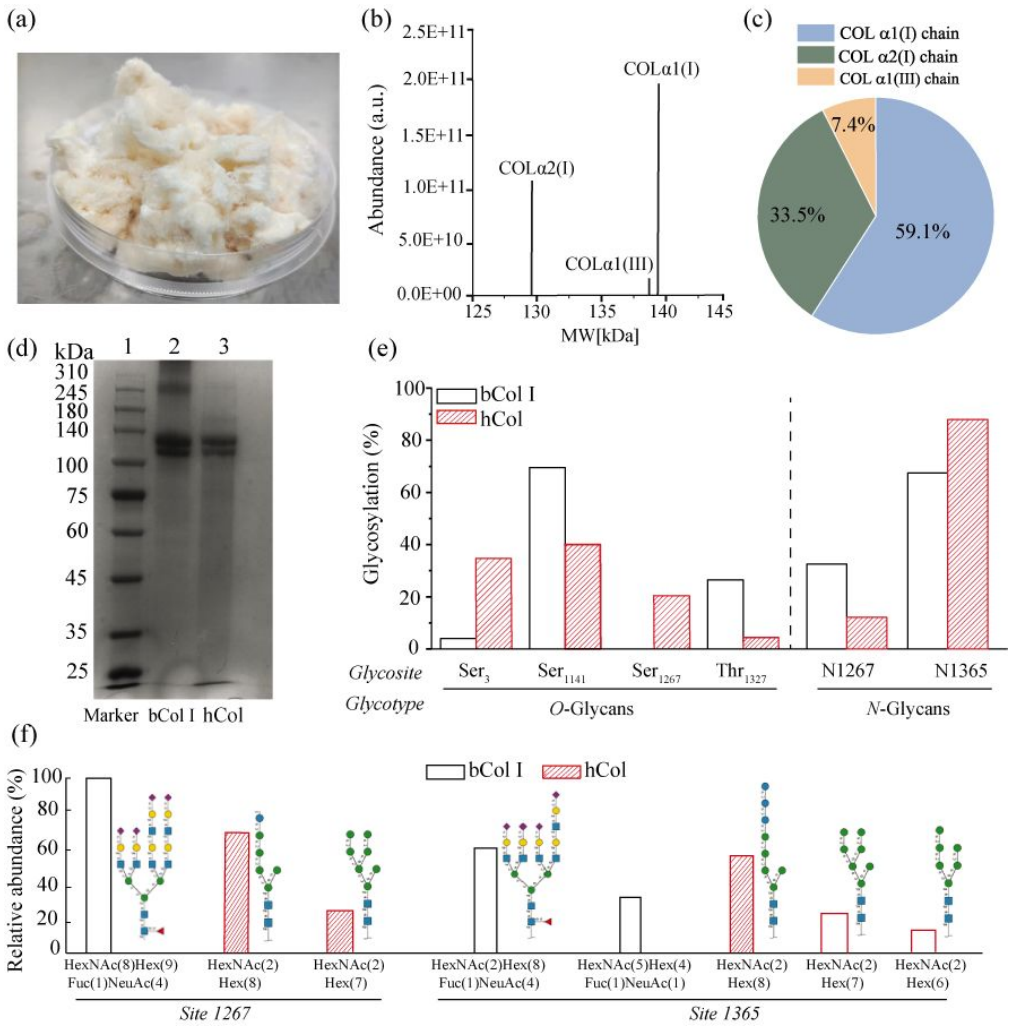

Figure 2. Biochemical characterization of hCol as compared to native bCol I. (a) The photo of purified massive hCol. (b). Mass spectrum of hCol as a function of molecular weight (MW). (c) Most abundance of collagen chain in hCol as detected by mass proteomics. (d) Protein gel electrophoresis of the collected human ECM-like collagen (hCol) from the PES scaffolds. Lane 1 is molecular weight ladder and lanes 2and 3 are from the samples of bCol and hCol. (e) The percentage of O-glycosites and N-glycosites in bCol I and hCol, respectively. (f) The relative abundance of N-glycan composition for N1267 and N1365 between bCol I and hCol (upper pannel: bCol I; lower pannel: hCol).

Before assembling into suprastructures, the inter-chain disulfide bonds between the C-propeptides of collagen are formed as in animals, which requires chain selection and collagen-specific molecular chaperones [32]. Therefore, the confirmation of the presence and location of the disulfide bond was obtained from the MS/MS spectrum

(Fig. S1). A series of b/y type ions from backbone cleavage between collagen α chains were both generated in bCol I and hCol (see Table 1). For α1 to α2 chain, ions with m/z of 74.06, 147.11 and 175.12 were detected for hCol while no valuable ion fragments were observed for bCol I. Nevertheless, 518.28 and 781.37 ions for bCol I as well as 102.06, 166.09, 215.10, 245.11, 385.21, 690.33, 713.89 and 718.84 ions for hCol, were all generated by the cleavage of disulfide bonds from the peptides that had same amino acid sequence (TCIRAQPE-VDIGPVCF). This confirmed the disulfide bond formed at the same site for two groups. Besides, the fragment ions from bCol I (m/z: 205.08, 212.10, 283.14, 662.34 and 725.34) and the ions from hCol (m/z: 175.12, 356.20 and 382.17) were both related to the same amino acid sequence (NPARTCR-FCHPE) with cysteines (Cys) connected vis S-S bond between α2 chain and α3 chain. Moreover, two groups also showed the same amino acid sequence (TCISANPLNVPR-DGCTKHTGE) within α3 chains, with Cys cleaved as indicated by m/z 387.20 for hCol as well as 74.06 ,102.06, 159.08 and 175.12 ions from bCol I. All disulfide linkages were formed at the same sites between α chains in hCol as in native bCol I, though the length of fragments were different.

3.3 Structural characterization of humanized ECM

3.3.1. Molecular structure of hCol

As seen in Fig 3a and Table S1, FTIR spectra of hCol and bCol I showed the same wavenumber of amide A and amide I, while exhibiting redshifts in amide B, amide II and amide III (predominantly N-H bending vibrations). These redshifts indicated a higher proportion of hydrogen bond for NH groups, which hold the collagen strands

Table 1. Ions observed in the spectra of disulfide peptide for bCol I and hCol

Group	Peptide sequence	Fragment ions	Assignment of fragment ions	Charge z	m/z
bCol I	TCIRAQPE-VDIGPVCF	AKNW	y4 (CoI α2 chain)	1+	518.28
		DIGGADQEFFVDIGE	b15 (CoI α1 chain)	2+	781.37
			β2 (CoI α3 chain)	1+	205.08
	NPARTCRDLR-FCHPE	NP	b2 (CoI α2 chain)	1+	212.10
		NPA	b3 (CoI α2 chain)	1+	283.14
		ELKSGE	y6 (CoI α3 chain)	1+	662.34
		CFC	b2 (CoI α3 chain)	2+	725.34
	CISANPLNVPR-DGCTKHTGE	GNSK	b4 (CoI α3 chain)	1+	387.20
hCol	DLKMCHSDWK-NPARTCRDLR	K	y1 (CoI α1 chain)	2+	74.06
		K	y1 (CoI α1 chain)	1+	147.11
		R	y1 (CoI α2 chain)	1+	175.12
	TCIRAQPE-VDIGPVCF	T	b1 (CoI α2 chain)	1+	102.06
		F	y1 (CoI α2 chain)	2+	166.09
		VD	b2 (CoI α2 chain)	1+	215.20
		PE	y2 (CoI α2 chain)	1+	245.11
		VDIG	b4 (CoI α2 chain)	1+	385.21
		PVCF	y4 (CoI α2 chain)	2+	690.33
		IRAQPE	y6 (CoI α2 chain)	1+	713.39
		GPVCF	y5 (CoI α2 chain)	2+	718.84
	NPARTCR-FCHPE	R	y1 (CoI α2 chain)	1+	175.12
		GSRKNP	b7 (CoI α2 chain)	2+	356.20
		HPE	y3 (CoI α3 chain)	1+	382.17
	CISANPLNVPR-DGCTKHTGE	K	y1 (CoI α3 chain)	2+	74.06
		T	b1 (CoI α3 chain)	1+	102.06
		TG	b2 (CoI α3 chain)	1+	159.08
		R	y1 (CoI α3 chain)	1+	175.12
		DGCT	b4 (CoI α3 chain)	2+	973.45

Note: Peptide sequence is the same sequence shared between hCol and bCol I.

together in hCol. The Amide III peak to $\upsilon(CH_2)$ peak (at 1450 cm^{-1}) ratio was usually used to determine the degree of unique secondary structure-triple helix, which was about 1.0 for native collagen [33]. Here, this ratio in hCol (0.98) was slightly lower than bCol I (1.0), suggesting a lower degree of triple helix structures in hCol as compared to native collagen. Furthermore, the secondary structure in detail was investigated using Raman spectroscopy and the characteristic peak assignments of bCol I and hCol in the region 600-1800 cm^{-1} were listed and explained in Table. S2. The spectra region of 600-1200 cm^{-1} in both spectra was dominated by S-S, C-S and C-C stretching of amino acids such as hydroxyproline, proline, tyrosine, cystine, tryptophan and phenylalanine (Fig. 3b). In particular, the presence of hydroxyproline peak at 816 cm^{-1} for hCol supported the hydroxylation of proline residues in collagen alpha chains, which can be required for the stability of the collagenous triple helix at physiological temperatures. For amide I band, it has been proven to be the most sensitive and popular band to study protein secondary structure, with each type of secondary structure correlated to a slightly different C=O stretching frequency due to its unique molecular geometry [34]. The amide I band was decomposed to show different secondary structures and amide I of hCol was dominated by the triple helix, with its abundance lower than that in bCol I (Fig. 3c and 3d), which was consistent with findings from FTIR investigations. After determining presence and abundance of triple helix structure, the thermal stability of triple helix structure was characterized

using cicular dichroism. Both bCol I and hCol showed the positive peak around 222 nm (Fig. 3e), indicating hCol had a similar triple helix structure as native bCol I. The melting behavior of triple helix was monitored by the change of ellipticity at 222nm and transition mid-temperature (T_m) due to denaturation of triple helix was obtained from the first derivatives of sigmoidal fitting of the melting curves. As shown in Fig. 3f, T_m of hCol was 35˚C and was slightly lower than that of bCol I (T_m= 36.6˚C), indicating slightly lower degree of conformational stability in hCol. Nevertheless, the degradation temperature for both bCol I and hCol was above 40˚C, suggesting stability of the triple helix structure of hCol under normal physiological conditions.

3.3.2 Morphology analysis of fibrillar structure in hCol

Fibrillar collagens, including type I and type III are higher order, supramolecular assemblies of triple helices to form fibril structures [35]. As shown in Fig. 4a, a dense crust of highly aligned fibrils was formed within fiber structures in hCol. As to well-distributed collagen fibrils in solution, a fibril with diameter of around 30 nm was observed (Fig.4b), which fell within the ranges of collagen fibril diameters reported in the literature (20-500 nm) [36]. Besides, alternate light/dark-band patterns were observed in the fibril of larger diameter (Fig.4c), which was associated with regular arrangement of the collagen monomers (termed D-period). Here, the measured D-period was around 68 nm, consistent with literature values for fibrillar collagen [19, 37]. The HAADF-STEM image of the fibril was applied with EDS analysis and strong peaks of carbon and nitrogen elements were observed in hCol (Fig.4d-4f). All above results demonstrated a native-like higher-order structures formed in hCol.

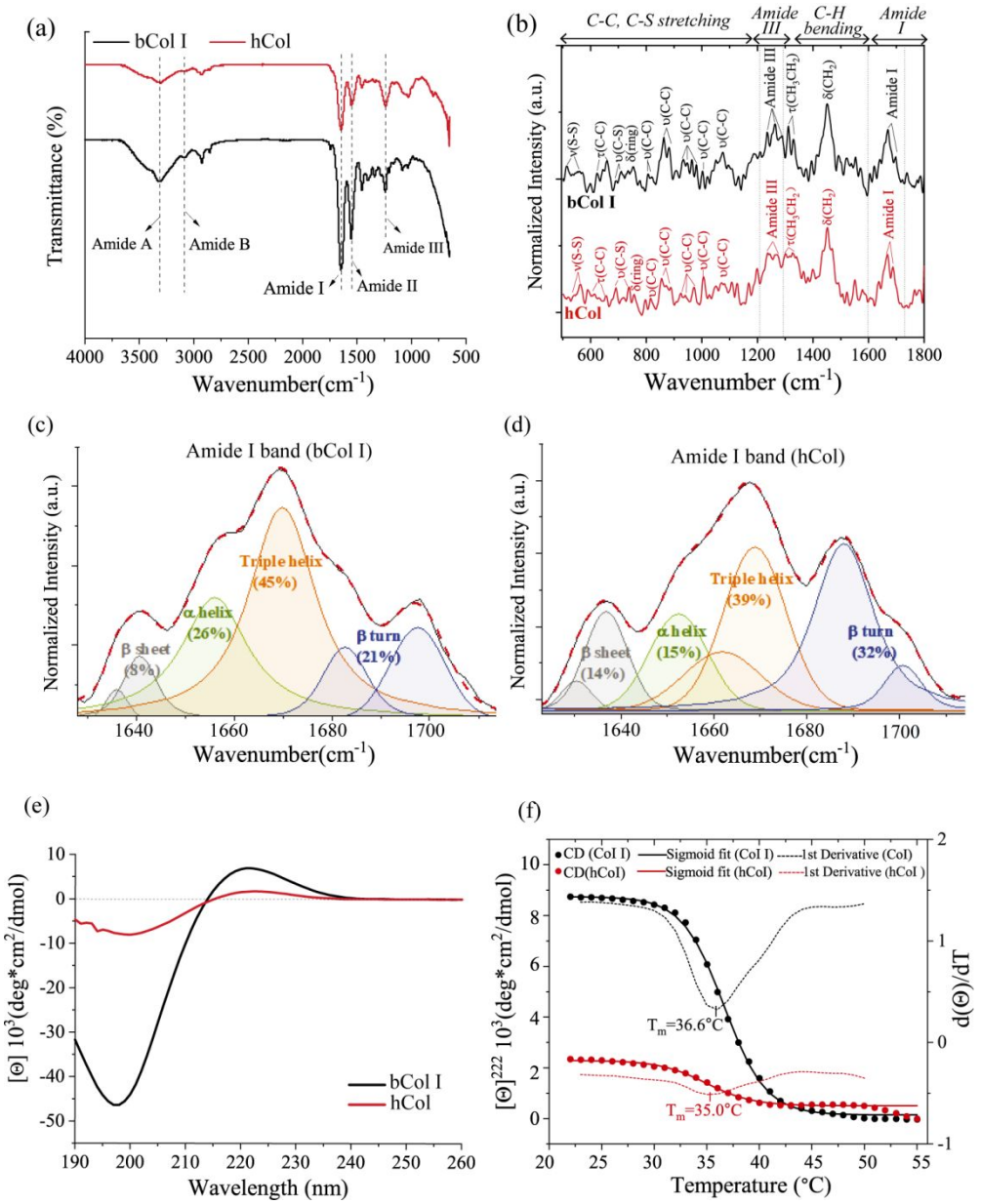

Figure 3. The molecular structure analysis of hCol and bCol I. (a) FTIR spectra and Raman spectra of bCol I and hCol. The decomposition of amide I Raman band for (c) bCol I and (d) hCol. (e) The CD spectra of bCol I and hCol at room temperature 22˚C. (f). Mean residue molar ellipticity at 222 nm [Θ], as a function of temperature for bCol I (black dot) and hCol (red dot) which is fitted with the sigmoid equation. The first derivatives from sigmoid fits were shown dashed lines.

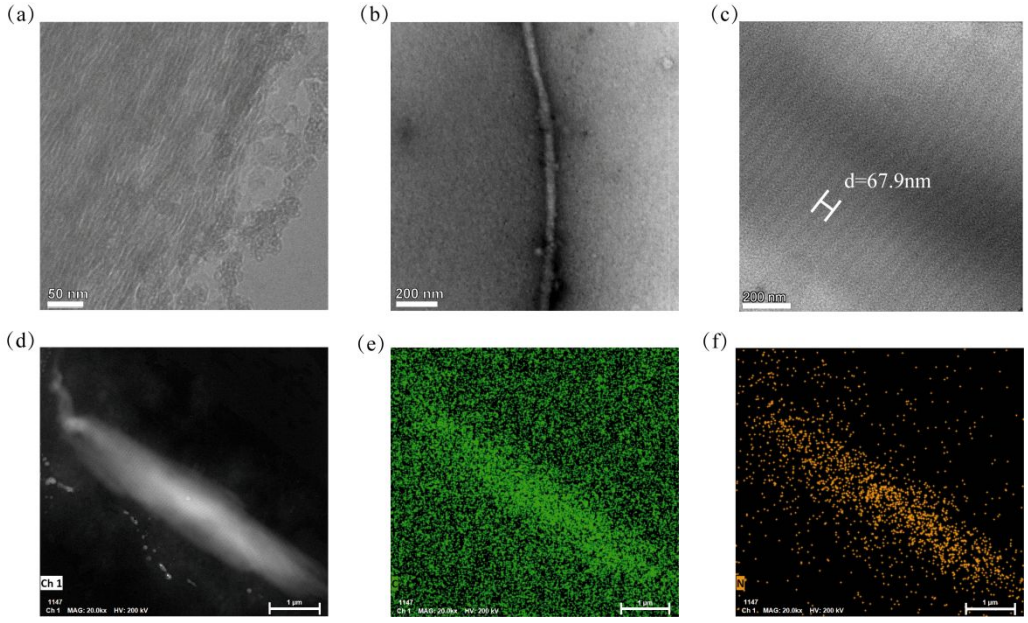

Figure. 4 The morphology analysis of fibril structure in hCol. TEM images of (a) a cluster of collagen fibrils, (b) individual fibril and (c) D-periodicity within fibrils. (d) The HAADF-STEM image and EDS mapping of the collagen fibril for (e) carbon element and (f) nitrogen element.

3.4 Influence of hCol on cell behaviors and cell phenotype

Collagen plays a important role in regulating cell bahaviors and phenotype, not only due to abundant cell recognition sites but also its unique structure form [38-40]. Cellular interactions with engineered collagen are largely affected by how closely the collagen is able to recapitulate the structure of native collagen on different length scale [41]. Multilevel hierarchical structures were observed in hCol, which might affect a series of biological cell behaviors, including proliferation, migration, differentiation and more.

First, the influence of hCol on cell viability and cell proliferation was evaluated using a CCK-8 assay and brightfield cell counting (Fig. 5a), respectively. As seen in Fig. 5b, the cell viability of hASCs indicated by absorbance at OD 450 nm increased with the addition of hCol in the cell medium (10μg/mL) compared to the blank control

(cell medium only) after 24h and 48h of seeding. The number of hASCs increased with culturing time and the significant difference in the cell number in hCol was greater compared to blank control (Fig. 5c). Besides, the effect of hCol on cell migration was detected by scrape motility assays. As seen in Fig. 5d and 5e, the scratching test showed that hASC migration rate was greater in hCol as compared to bCol I and blank control. The collagen structure has been experimentally shown to influence cell migration, which might get side-lined without its triple helix and fibrillar structure [42, 43]. Hereby, to test if this is related to the native-like structure of collagen, the cell migration was investigated for hCol with different treatments. Except alkali-treated hCol, the migration rate was lower in the all treatment groups as compared to no-treatment (Fig. 5f). Furthermore, to analyze the effect of hCol on cell phenotype, Oil red O staining was used to indicate adipogenic differentiation. The hASCs cultured in control expansion medium did not undergo adipogenesis, which did not stain positive with Oil Red O (Fig. 5g). The hASCs cultured in AIM differentiation medium were differentiated, showing positive Oil red O staining. The cells seeded on hCol-coated surface in AIM medium were differentiated and more and bigger lipid droplets were detected as compared to AIM group. AIM+hCol group yielded higher percentages of lipid-positive cells, with significant differences as compared to AIM (Fig. 5h). When hASCs differentiate into adipocytes, several differentiation-linked genes are activated, among which lipoprotein lipase (LPL) and peroxisome proliferator-activated receptor γ2 (PPARγ2) are important genes induced in the adipogenic differentiation process. The differentiation in AIM+hCol group

showed expression of LPL by 2-fold increased and expression of PPARγ2 by 2 fold increased as compared to AIM group (Fig. 5i and 5j).

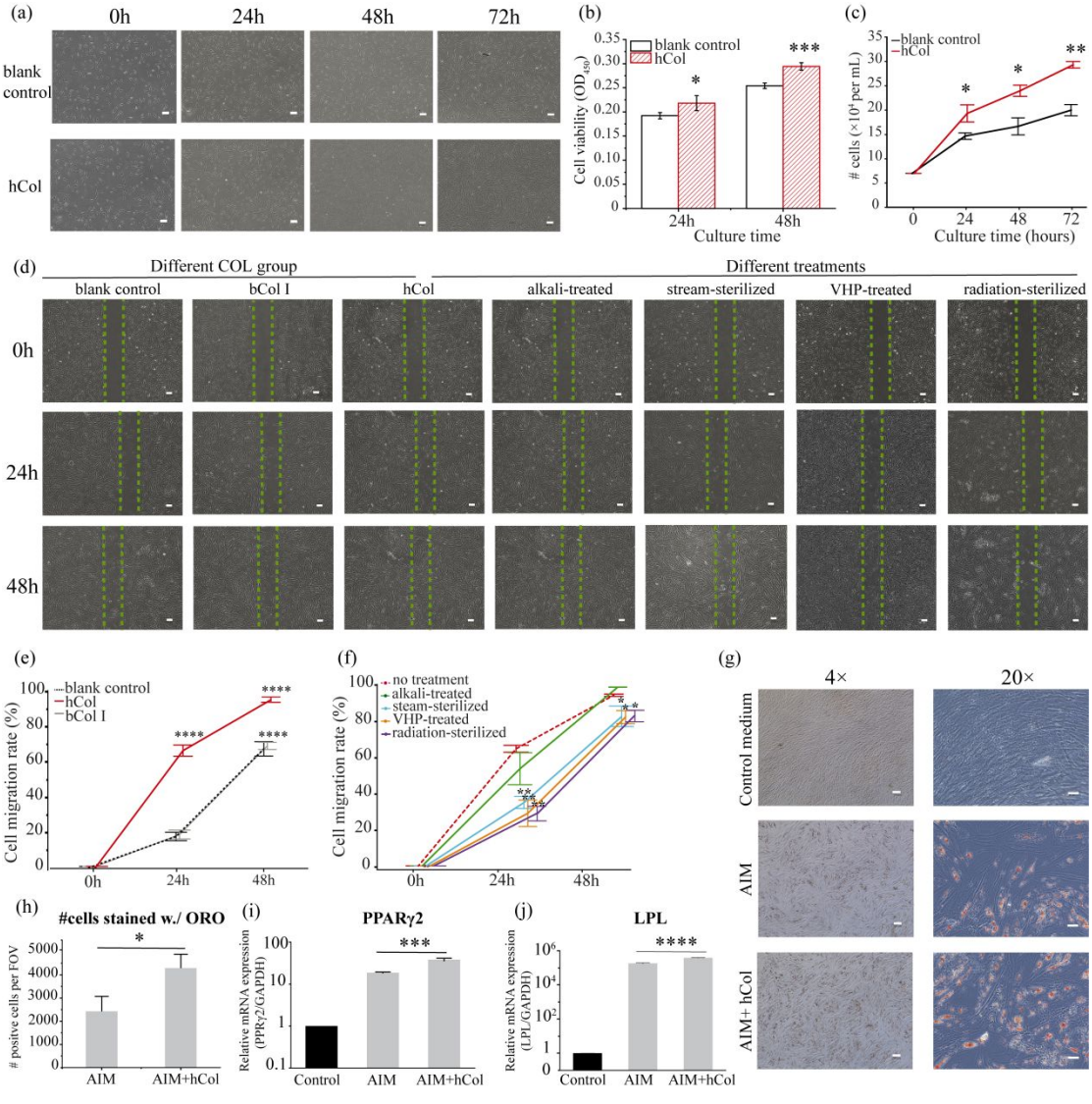

Figure. 5 hCol promotes cell proliferation, cell migration and adiopenesis of hASC. (a) Representative images show cell confluency at different times (blank control: complete growth medium alone; AIM: adipogenic induction medium alone; AIM+ hCol: seeded on hCol-coated surface in AIM medium), scale bar =200μm. (b) CCK-8 assay: OD450 absorbance in hASCs cells (mean ± SD, n=4). (c) Cell growth curve determined by cell count after 0, 24, 48, and 72 h of hASC cells exposure to hCol media (mean±SD, n=3). (d) Representative images of cell migration in different collagen (COL) groups and different treatment groups, scale bar=50μm. (e) The cell migration rate of different COL groups (means ± SD, n=3). (f) The migration rate of cells exposure to hCol with different treatments (means ± SD, n=2). (g) The

representative images of Oil Red O staining of hASC (4 × : scale bar=200μm; 20 × : scale bar= 50μm). (h) The quantified result for oil red O-positive hASCs cultured in control growth media, AIM and AIM+hCol. And the relative expression of (i) LPL and (j) PPARγ2 gene normalized to GAPDH mRNA expression. (mean±SD, n=3). Statistical difference: *p < 0.05, **p < 0.01, *** p<0.001and ****p<0.0001 as compared with blank control at each time point.

3.5 The effect of hCol on wound healing

Collagen, as a bioactive component *in vitro*, has been exploring in wound care supplement for post-treatments to provide microenvironment for cell growth and promoting matrix remodeling [44]. Hereby, a full-thickness wound area was created on tail skin per mouse (post- operative day 0) and wound closure was measured by the area of the wound bed over time, normalized to the initial wound after treatment (Fig. 6a). As seen in the photos of wound areas, the mice of hCol group healed more quickly as compared to the commercial control. Specifically, the wound closure values for hCol (n = 3) versus control (n = 3) mice were 79% versus 3% at day 7(P < 0.05), 76% versus 56% at day 14 (P < 0.05) and 55% versus 26% at day 21 (P<0.01) in Fig. 6b. For the late stage of wound healing, hCol showed epidermis regeneration and healthy dermis with no inflammation, while control group displayed inflammation in the regenerated epidermis at day 14. At day 21, hCol displayed a uniform thickness of newly generated epidermis while control group did not (Fig. 6c).

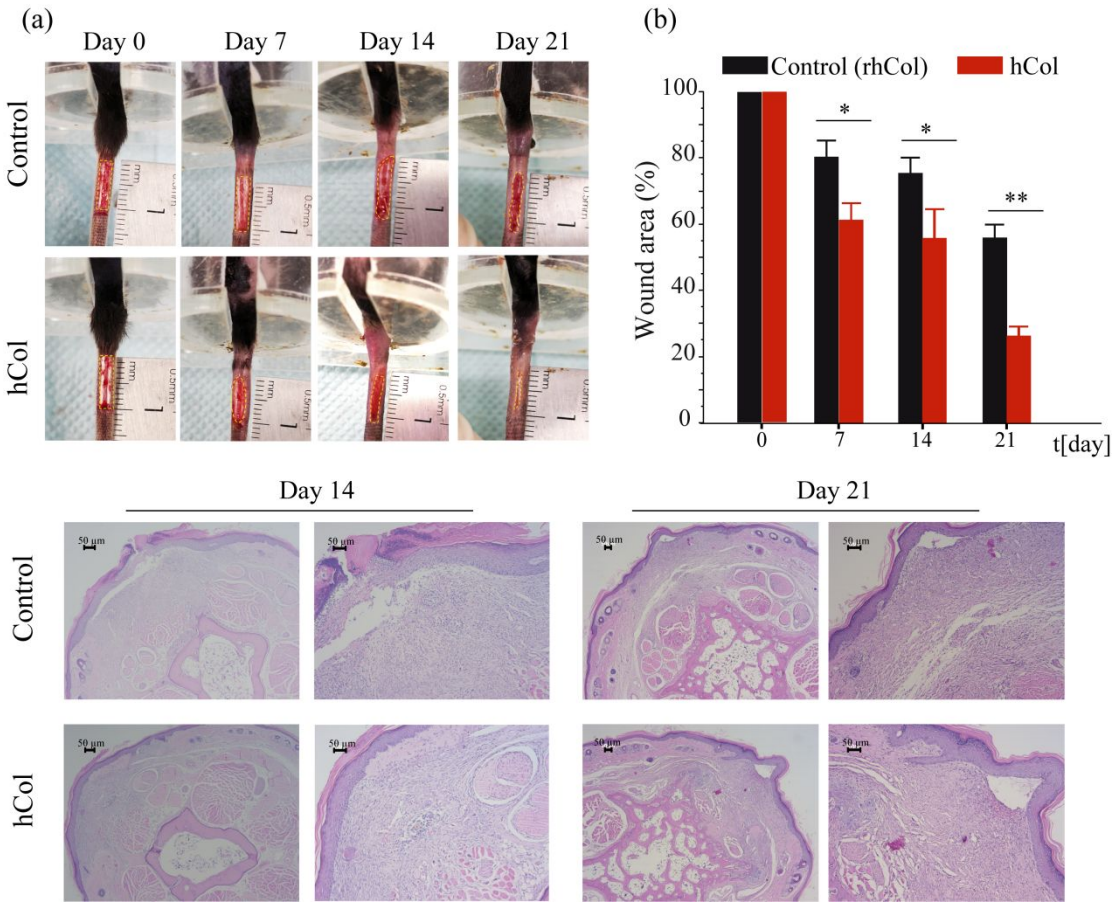

Figure. 6 The effect of hCol on wound healing in mouse tail skin. (a) Representative photographs of mouse tail skin days 0, 7, 14 and 21 after wounding (control: commercial collagen). (b) The quantified wound closure area normalized to day 0 post-operation. (c) Hematoxylineosin (HE) staining of cross-section of mouse tail 14 days and 21 days after operation. All bars shown in (b) represents mean ± SD (n=3, hCol; n=3,control). * $P < 0.05$; **$P<0.01$ versus control at each time point.

4. Discussion

Each collagen α chain consists of 3 domains: N-propeptide, uninterrupted triple helix and C-telopeptide [45, 46]. The specific glycosylated hydroxylysine residues (O-linked glycosylation) are formed in the triple helix region of proα chains [47]. Each chain of C-propeptide is glycosylated by high-mannose asparagine-linked oligosaccharide (N-glycosylation) and this domain is further stabilized by interchain-disulfide bonds [48]. After these and other modifications, two proα1 chains

and one proα2 chain are folded into a triple helix structure from the C- to the N-terminus [49]. Subsequent to folding, an offset, parallel packing of triple-helices is generated to form microfibrils [50]. The three-dimensional structure is featured by a 67 nm D-periodic repeat [51]. The hierarchical packing structure is maintained *in vivo* through the attachment of stabilizing ligands to both the fibril and fibril-bundle(s) [52]. Due to its bioactive domains and unique hierarchical structures at different length scales, collagen plays a dominant role in regulating cell function and directing tissue development [43, 53]. Therefore, the components and multi-scale structures of hCol were verified by SDS-PAGE, HPLC-MS, FTIR, Raman, CD spectroscopy, SEM and TEM in this work to confirm its native-like properties.

To collect hCol, cells and PES materials were removed and from SEM images, the microstructure of ECM was still complete after the treatment. The SDS-PAGE analysis showed high purity of type I collagen in hCol. HPLC-MS further demonstrated glycosylation and disulfide linkages occurred at the same sites on collagen alpha chains in hCol as compared to native bCol I. This implied hCol had correct post-translational modifications and folding of domains prior to triple helix formation as compared to native bCol I. Although the N-glycan structure was different between hCol and bCol I, it could result from different features of N-glycosylation in the two groups [54, 55]. The cell culture process could also influence N-glycosylation structure of proteins derived from cells [56, 57]. In the future, cell culture process should be well controlled regarding to N-gycosylation structures in human native collagen. For collagen assembling into a triple helix

structure, FTIR spectra displayed a lower degree of triple helix in hCol , which was in parallel to the CD spectroscopy results where thermal stability of triple helix structure in hCol was slightly lower than bCol I. This may imply a slightly different peptide sequence, length, and modifications in collagen for hCol I and bCol. Nevertheless, the degradation temperature of the triple helix in hCol was above normal physiological temperature, indicating hCol had capability to maintain its function in human body. More importantly, Raman spectra showed the predominance of triple helix structure in hCol along with other secondary structures such as alpha helix and beta sheet. The globular heads in C1 domain of collagen chain primarily contains beta-sheet structure and type III collagen has a lower alpha helix and triple helix than type I.[58] Hence, it could result in a smaller percentage of alpha and triple helix in hCol with a certain amount of type III collagen as seen in Fig. 3c and 3d. For other regions, although the Raman positions of peaks in C-C, C-S stretching region, amide III and C-H bending position were different to some degree between bCol I and hCol, it could attribute to spectral variability and broad spectral features in biological samples [59, 60]. For fibrillar structure, SEM and TEM showed a 68nm D-periodicity of collagen fibril in hCol. This banded structure results from the axial stagger of adjacent tropocollagen molecules, recorded as gap and overlap regions. The regular array of gap and overlap regions indicated regular assembly of collagen monomers formed in hCol. Overall, type I collagen was predominant in hCol with a few amount of type III collagen, which was similar to the composition of human body with less than 20% of type III collagen.

After confirming native-like structural features in hCol, the effects of hCol on cell behavior and phenotype were examined. As one of the ideal candidates for use in regenerative medicine protocols, hASCs have the capability to differentiate into a particular lineage cells that replace damaged cells and contribute to tissue regeneration [61]. However, the successful use of MSC in therapy requires developing well-defined methods for cell growth and directing differentiation [62]. These results showed hCol promoted hASC viability, proliferation and migration. The migration ability was greater for hCol than bCol I, which could result from a higher content of integrin recognition sequences in hCol than bCol I, leading to a higher probability of interacting with hASC integrins. Meanwhile, collagen triple helices as guidance structures for contacting cells, the degradation of triple helix structure resulted in reduced migration ability [63]. In this work, heating, hydrogen peroxide and radiation treatment can cleave the hydrogen and covalent bonds to destabilize the triple helix of hCol, which suppressed the cell migration ability. However, alkaline treatment had less effect on the triple helix structure of collagen as previously reported in the several literatures [64, 65]. The alkaline treatment can remove the telopeptides of the collagen molecules and break off additional crosslinking in the triple helical regions without damaging the integrity of the triple helix, which can retain the integrin recognition sites for binding cells without much impact on cell migration as compared to no-treatment. Besides, hCol promoted adipocyte differentiation as compared to hASCs cultured in adipogenic induction media by a higher number of mature adipocytes through enhanced expression of LPL

and PPARγ2 genes that play an important role in adipocyte differentiation. Moreover, hCol can accelerate cutaneous wound healing as compared to commercial recombinant collagen product by causing less inflammation as seen in the HE staining images. The could be due to the more native-like property of hCol compared to recombinant collagen, as hCol was directly derived by cell *in vitro* that contained all necessary domains for bioactivity. Whether the healing capability is related to native triple helix structure of hCol should be investigated in future. Meanwhile, several studies have demonstrated that type I collagen promoted cell migration, cell attachment and MSC adipogenesis by more cell to cell surface contact points and interaction with cellular receptors (e.g. α2β1, DDR2, etc.) [1, 17]. All of these suggest that a platform to produce native-like collagen from cell-derived matrix was provided and hCol could be potentially used as *in vitro* cell culture model in tissue engineering or cosmetics [66]. In future, the mechanism of how collagen structure promotes cell phenotype and skin repair needs to be investigated in combination with more molecular biology tests.

5. Conclusion

The biochemical characterization in this study verified a high purity of type I collagen in hCol. The structural examinations at different length scales confirmed native-like hierarchical structures in hCol, consisting of triple helix structures with the native form of post-translational modification, assembled into supramolecular fibrils with banded 68 nm repeating structures. The *in vitro* cell culture with hCol indicated its

noticeable influence on hASC behaviors and phenotype, including promoting cell proliferation, migration and hASC adipogenesis. Besides, hCol also accelerated cutaneous wound closure compared to available commercial collagen products, implying that hCol can serve as a prospective candidate for tissue repair as native collagen. This study can provide a strategy to harvest native-like collagen and gives detailed evidence to fill in the knowledge gap of structure and its effect on cell behaviors, which might support its application in tissue repair.

Declaration of Competing Interest

The authors declare that they have no known competing financial interests or personal relationships that could have appeared to influence the work reported in this paper.

Acknowledgements

The authors acknowledge support form the National Key R&D Program of China (2021YFB3800705), the Science and Technology Innovation Program of Hunan Province (2022RC4013) and the Science and Technology Program of Changsha (kq2303005).

References

1. Heino J. The collagen family members as cell adhesion proteins. *Bioessays* 2007;29:1001-10.
2. Hadjipanayi E, Mudera V, Brown RA. Guiding cell migration in 3D: a collagen matrix with graded directional stiffness. *Cell Motil Cytoskeleton* 2009;66:121-8.

3. Glowacki J, Mizuno S. Collagen scaffolds for tissue engineering. *Biopolymers* 2008;89:338-44.
4. Wang H. A Review of the Effects of Collagen Treatment in Clinical Studies. *Polymers (Basel)* 2021;13.
5. Dong L, Liu Q, Gao Y, Jia H, Dai W, Guo L, Fan H, Fan Y, Zhang X. The effect of collagen hydrogels on chondrocyte behaviors through restricting the contraction of cell/hydrogel constructs. *Regen Biomater* 2021;8:rbab030.
6. Kanta J. Collagen matrix as a tool in studying fibroblastic cell behavior. *Cell Adh Migr* 2015;9:308-16.
7. Browne S, Zeugolis DI, Pandit A. Collagen: finding a solution for the source. *Tissue Eng Part A* 2013;19:1491-4.
8. Addad S, Exposito JY, Faye C, Ricard-Blum S, Lethias C. Isolation, characterization and biological evaluation of jellyfish collagen for use in biomedical applications. *Mar Drugs* 2011;9:967-983.
9. F.Ruggiero JYE, P. Bournat, V. Gruber, S.Perret, J. Comte, B. Olagnier, R. Garrone and M. Theisen. Triple helix assembly and processing of human collagen produced in transgenic tobacco plants. *the Federation of European Biochemical Societies letter* 2000:132-136.
10. Rutschmann C, Baumann S, Cabalzar J, Luther KB, Hennet T. Recombinant expression of hydroxylated human collagen in Escherichia coli. *Appl Microbiol Biotechnol* 2014;98:4445-55.
11. Ishikawa Y, Bachinger HP. A molecular ensemble in the rER for procollagen maturation. *Biochim Biophys Acta* 2013;1833:2479-91.
12. Li RC, Wong MY, DiChiara AS, Hosseini AS, Shoulders MD. Collagen's enigmatic, highly conserved N-glycan has an essential proteostatic function. *Proc Natl Acad Sci U S A* 2021;118.
13. Wang X, Lu Y, Wang W, Wang Q, Liang J, Fan Y, Zhang X. Effect of different aged cartilage ECM on chondrogenesis of BMSCs in vitro and in vivo. *Regen Biomater* 2020;7:583-595.
14. Gao C-Y, Wang G, Wang L, Wang Q-S, Wang H-C, Yu L, Liu J-X, Ding J-D. A Biosurfactant-containing TSD Strategy to Modify Bovine Pericardial Bioprosthetic Valves for Anticalcification. *Chinese Journal of Polymer Science* 2022;41:51-66.
15. Xing H, Lee H, Luo L, Kyriakides TR. Extracellular matrix-derived biomaterials in engineering cell function. *Biotechnol Adv* 2020;42:107421.
16. Zhang WM, Kapyla J, Puranen JS, Knight CG, Tiger CF, Pentikainen OT, Johnson MS, Farndale RW, Heino J, Gullberg D. alpha 11beta 1 integrin recognizes the GFOGER sequence in interstitial collagens. *J Biol Chem* 2003;278:7270-7.
17. Farndale RW. Collagen-binding proteins: insights from the Collagen Toolkits. *Essays Biochem* 2019;63:337-348.
18. Tzaphlidou M. Measurement of the axial periodicity of collagen fibrils using an image processing method. *Micron* 2001;32.
19. Stylianou A. Assessing Collagen D-Band Periodicity with Atomic Force Microscopy. *Materials (Basel)* 2022;15.

20. Malcor JD, Hunter EJ, Davidenko N, Bax DV, Cameron R, Best S, Sinha S, Farndale RW. Collagen scaffolds functionalized with triple-helical peptides support 3D HUVEC culture. *Regen Biomater* 2020;7:471-482.
21. Wang Z-Y, Zhang X-W, Ding Y-W, Ren Z-W, Wei D-X. Natural biopolyester microspheres with diverse structures and surface topologies as micro-devices for biomedical applications. *Smart Materials in Medicine* 2023;4:15-36.
22. Kornmuller A, Brown CFC, Yu C, Flynn LE. Fabrication of Extracellular Matrix-derived Foams and Microcarriers as Tissue-specific Cell Culture and Delivery Platforms. *J Vis Exp* 2017.
23. Zhao XH, Peng XL, Gong HL, Wei DX. Osteogenic differentiation system based on biopolymer nanoparticles for stem cells in simulated microgravity. *Biomed Mater* 2021;16.
24. Su S, Qiu Y, Shi X, Zhou T, Wang P, Xiao E, Wei Q, Zhao C. Phase Separation Microparticles as a Three-Dimensional Cell Culture System To Promote Stem Cell Expansion. *Biomacromolecules* 2023;24:2184-2195.
25. Wei DX, Dao JW, Chen GQ. A Micro-Ark for Cells: Highly Open Porous Polyhydroxyalkanoate Microspheres as Injectable Scaffolds for Tissue Regeneration. *Adv Mater* 2018;30:e1802273.
26. Xiao E. Extracellular Matrix MB Bioprotein and Its Preparation Reagents Kit and Method (Patent No. CN112538513B). *China Patent and Trademark Office* 2020.
27. Amirrah IN, Lokanathan Y, Zulkiflee I, Wee M, Motta A, Fauzi MB. A Comprehensive Review on Collagen Type I Development of Biomaterials for Tissue Engineering: From Biosynthesis to Bioscaffold. *Biomedicines* 2022;10.
28. Chang CC, Chow CC, Tellier LC, Vattikuti S, Purcell SM, Lee JJ. Second-generation PLINK: rising to the challenge of larger and richer datasets. *Gigascience* 2015;4:7.
29. Zhou H, Llanes JP, Lotfi M, Sarntinoranont M, Simmons CS, Subhash G. Label-Free Quantification of Microscopic Alignment in Engineered Tissue Scaffolds by Polarized Raman Spectroscopy. *ACS Biomater Sci Eng* 2023;9:3206-3218.
30. Suarez-Arnedo A, Torres Figueroa F, Clavijo C, Arbelaez P, Cruz JC, Munoz-Camargo C. An image J plugin for the high throughput image analysis of in vitro scratch wound healing assays. *PLoS One* 2020;15:e0232565.
31. Zhang Y, Chen Y, Zhao B, Gao J, Xia L, Xing F, Kong Y, Li Y, Zhang G. Detection of Type I and III collagen in porcine acellular matrix using HPLC-MS. *Regen Biomater* 2020;7:577-582.
32. Widmer C, Gebauer JM, Brunstein E, Rosenbaum S, Zaucke F, Drogemuller C, Leeb T, Baumann U. Molecular basis for the action of the collagen-specific chaperone Hsp47/SERPINH1 and its structure-specific client recognition. *Proc Natl Acad Sci U S A* 2012;109:13243-7.
33. Veeruraj A, Arumugam M, Ajithkumar T, Balasubramanian T. Isolation and characterization of collagen from the outer skin of squid (Doryteuthis singhalensis). *Food Hydrocolloids* 2015;43:708-716.
34. Nakul C. Maiti MMA, Michael G. Zagorski, Paul R. Carey and Vernon E. Anderson. Raman Spectroscopic Characterization of Secondary Structure in Natively

Unfolded Proteins: r-Synuclein. *Journal of the American Chemical Society* 2004;126:2399-2408.
35. Yi K, Li Q, Lian X, Wang Y, Tang Z. Utilizing 3D bioprinted platelet-rich fibrin-based materials to promote the regeneration of oral soft tissue. *Regen Biomater* 2022;9:rbac021.
36. Gautieri A, Vesentini S, Redaelli A, Buehler MJ. Hierarchical structure and nanomechanics of collagen microfibrils from the atomistic scale up. *Nano Lett* 2011;11:757-66.
37. Madhurapantula RS, Orgel JPRO. X-Ray Diffraction Detects D-Periodic Location of Native Collagen Crosslinks In Situ and Those Resulting from Non-Enzymatic Glycation. In: *Accelerator Physics - Radiation Safety and Applications*, 2018.
38. Shiamalee Perumal OA, and Joseph P. R. O. Orge. Collagen fibril architecture, domain organization, and
triple-helical conformation govern its proteolysis. *The National Academy of Sciences of the USA* 2008;105:2824–2829.
39. F. Gobeaux EB, G. Mosser, P. Davidson, P. Panine and M.-M. Giraud-Guille. Cooperative Ordering of Collagen Triple Helices in the Dense State. *Langmuir* 2007;23:6411-6417.
40. Koide T. Designed triple-helical peptides as tools for collagen biochemistry and matrix engineering. *Philos Trans R Soc Lond B Biol Sci* 2007;362:1281-91.
41. Salvatore L, Gallo N, Natali ML, Terzi A, Sannino A, Madaghiele M. Mimicking the Hierarchical Organization of Natural Collagen: Toward the Development of Ideal Scaffolding Material for Tissue Regeneration. *Front Bioeng Biotechnol* 2021;9:644595.
42. Zanotelli MR, Goldblatt ZE, Miller JP, Bordeleau F, Li J, VanderBurgh JA, Lampi MC, King MR, Reinhart-King CA. Regulation of ATP utilization during metastatic cell migration by collagen architecture. *Mol Biol Cell* 2018;29:1-9.
43. Goldberga I, Li R, Duer MJ. Collagen Structure-Function Relationships from Solid-State NMR Spectroscopy. *Acc Chem Res* 2018;51:1621-1629.
44. Gould LJ. Topical Collagen-Based Biomaterials for Chronic Wounds: Rationale and Clinical Application. *Advances in Wound Care* 2016;5:19-31.
45. Gordon MK, Hahn RA. Collagens. *Cell Tissue Res* 2010;339:247-57.
46. Hu J, Li J, Jiang J, Wang L, Roth J, McGuinness KN, Baum J, Dai W, Sun Y, Nanda V, Xu F. Design of synthetic collagens that assemble into supramolecular banded fibers as a functional biomaterial testbed. *Nature Communications* 2022;13.
47. Yamauchi M, Sricholpech M. Lysine post-translational modifications of collagen. *Essays Biochem* 2012;52:113-33.
48. Lamande SR, Bateman JF. The type I collagen pro alpha 1(I) COOH-terminal propeptide N-linked oligosaccharide. Functional analysis by site-directed mutagenesis. *J Biol Chem* 1995;270:17858-65.
49. Xu J, Luo X, Zhang Y, Gao J, Huang CC, Bai X, Zhang G. Extraction and characterization of bovine collagen Type V and its effects on cell behaviors. *Regen Biomater* 2022;9:rbac028.

50. Tang Y, Wang Z, Xiang L, Zhao Z, Cui W. Functional biomaterials for tendon/ligament repair and regeneration. *Regen Biomater* 2022;9:rbac062.
51. Birk DE, Bruckner P. Collagen Suprastructures. In: *Collagen*, 2005, 185-205.
52. Orgel JP, San Antonio JD, Antipova O. Molecular and structural mapping of collagen fibril interactions. *Connect Tissue Res* 2011;52:2-17.
53. Chen Q, Pei Y, Tang K, Albu-Kaya MG. Structure, extraction, processing, and applications of collagen as an ideal component for biomaterials - a review. *Collagen and Leather* 2023;5.
54. Behrens AJ, Duke RM, Petralia LM, Harvey DJ, Lehoux S, Magnelli PE, Taron CH, Foster JM. Glycosylation profiling of dog serum reveals differences compared to human serum. *Glycobiology* 2018;28:825-831.
55. Ashwood C, Waas M, Weerasekera R, Gundry RL. Reference glycan structure libraries of primary human cardiomyocytes and pluripotent stem cell-derived cardiomyocytes reveal cell-type and culture stage-specific glycan phenotypes. *J Mol Cell Cardiol* 2020;139:33-46.
56. Nam JH, Zhang F, Ermonval M, Linhardt RJ, Sharfstein ST. The effects of culture conditions on the glycosylation of secreted human placental alkaline phosphatase produced in Chinese hamster ovary cells. *Biotechnol Bioeng* 2008;100:1178-92.
57. Hossler P, Khattak SF, Li ZJ. Optimal and consistent protein glycosylation in mammalian cell culture. *Glycobiology* 2009;19:936-49.
58. Belbachir K, Noreen R, Gouspillou G, Petibois C. Collagen types analysis and differentiation by FTIR spectroscopy. *Anal Bioanal Chem* 2009;395:829-37.
59. Zhou H, Simmons CS, Sarntinoranont M, Subhash G. Raman Spectroscopy Methods to Characterize the Mechanical Response of Soft Biomaterials. *Biomacromolecules* 2020;21:3485-3497.
60. Butler HJ, Ashton L, Bird B, Cinque G, Curtis K, Dorney J, Esmonde-White K, Fullwood NJ, Gardner B, Martin-Hirsch PL, Walsh MJ, McAinsh MR, Stone N, Martin FL. Using Raman spectroscopy to characterize biological materials. *Nat Protoc* 2016;11:664-87.
61. Liu X, He J, Zhang S, Wang XM, Liu HY, Cui FZ. Adipose stem cells controlled by surface chemistry. *J Tissue Eng Regen Med* 2013;7:112-7.
62. Cao Y, Cheng P, Sang S, Xiang C, An Y, Wei X, Shen Z, Zhang Y, Li P. Mesenchymal stem cells loaded on 3D-printed gradient poly(epsilon-caprolactone)/methacrylated alginate composite scaffolds for cartilage tissue engineering. *Regen Biomater* 2021;8:rbab019.
63. Somaiah C, Kumar A, Mawrie D, Sharma A, Patil SD, Bhattacharyya J, Swaminathan R, Jaganathan BG. Collagen Promotes Higher Adhesion, Survival and Proliferation of Mesenchymal Stem Cells. *PLoS One* 2015;10:e0145068.
64. Shunji Hattori EA, Tetsuya Ebihara, Tomoko Shirai, Iori Someki and Shinkichi Irie. Alkali-Treated Collagen Retained the Triple Helical Conformation and the Ligand Activity for the Cell Adhesion via α2β1 Integrin. *The Journal of Biochemistry* 1999;125:676-684.

65. Meng D, Tanaka H, Kobayashi T, Hatayama H, Zhang X, Ura K, Yunoki S, Takagi Y. The effect of alkaline pretreatment on the biochemical characteristics and fibril-forming abilities of types I and II collagen extracted from bester sturgeon by-products. *Int J Biol Macromol* 2019;131:572-580.
66. Liu J, Zhou Z, Li H, Yang X, Wang Z, Xiao J, Wei D-X. Current status and challenges in the application of microbial PHA particles. *Particuology* 2024;87:286-302.

Supplementary materials

Human Extracellular Matrix (ECM)-like Collagen and its Bioactivity

Hui Zhou[1], Wenwei Li[2], Lixin Pan[2], Tianci Zhu[2], Teng Zhou[2], E Xiao[2*] and Qiang Wei[1,2*]

1. State Key Laboratory of Polymer Materials and Engineering, College of Polymer Science and Engineering, Sichuan University, Chengdu 610065, China

2. Hunan Maybio Bio-Pharmaceutical Co., Ltd., Changsha 410000, China

*Address correspondence to:wei@scu.edu.cn(Q.W.); xiaoe1986@vip.163.com(E.X.)

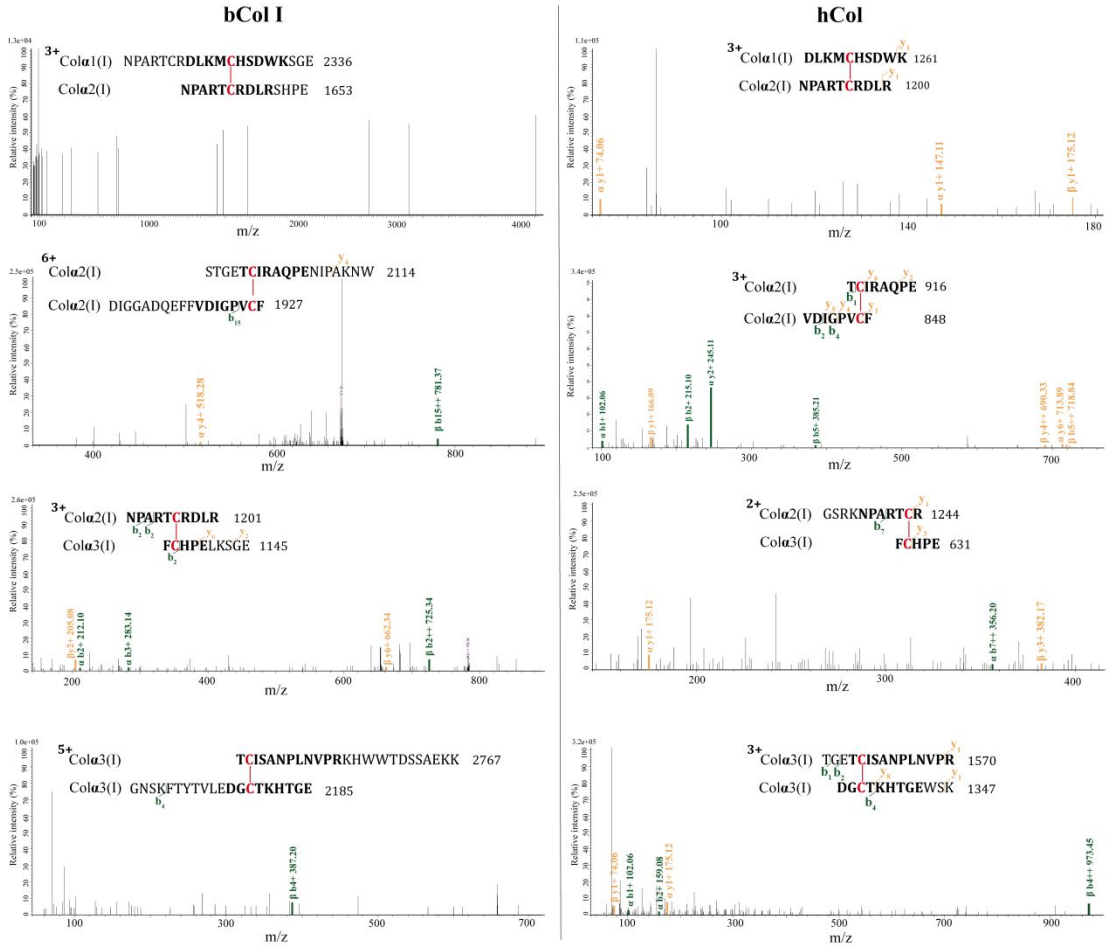

Fig S1. High similarity in sequencing positioning of disulfide linkages between bCol I and hCol. HCD spectra of different charge disulfide-linked peptide ions for bCol I and hCol resulting between collagen α1 and α2 chain(first row), α2 chains(second row), α2 to α3 chain(third row) and α3 chains(last row). The annotation in green and orange color denote fragments from the cleavage of amide bonds that retain N-terminus and C-terminus respectively.

Table S1. The major peak assignment in FTIR spectra of bCol I and hCol

Region	Peak wavenumber (cm^{-1})		Assignment
	bCol I	hCol	
Amide A	3313	3313	υ(C=O), υ(N-H)
Amide B	3091	3086	υ(N-H)
Amide I	1650	1650	υ(C=O)
Amide II	1549	1545	δ(N-H), υ(C-N)
Amide III	1239	1238	δ(N-H), υ(C-N)

Table S2. Raman characteristic band assignment in bCol I and hCol

Region	Peak wavenumber (cm^{-1})		Assignment
	bCol I	hCol	
υ(C-S), υ(C-C) & υ(S-S)	515, 564	520, 564	υ(S-S) of collagen
	624, 659	613, 657	τ(C-C) of cystine, tyrosine, phenylalanine (type I collagen)
	690, 735	690,737	υ(C-S) of proteins
	753	757	δ(ring) of tryptophan
	806, 820	796, 816	υ(C-C) of proline, tyrosine, hydroxyproline (collagen)
	863, 881	855, 887	υ(C-C) of proline, tyrosine and δ(ring) of tryptophan
	932, 946, 964, 980	924, 940, 972	υ(C-C) of proline, valine and protein backbone
	1002	1007	υ(C-C) of phenylalanine
	1075	1070, 1079	υ(C-C) of skeletal backbone in lipid
Amide III	1236, 1263, 1287	1237, 1245 1273	δ(N-H), υ(C-N) of glycine backbone & proline side chains
CH bending	1310, 1330	1300, 1328	τ(CH_2), τ(CH_3), ω(CH_2CH_3) of collagen
	1451	1452	δ(CH_2), τ(CH_2CH_3) of proteins
Amide I	1668, 1696	1667, 1688	υ(C=O) amide I of collagen

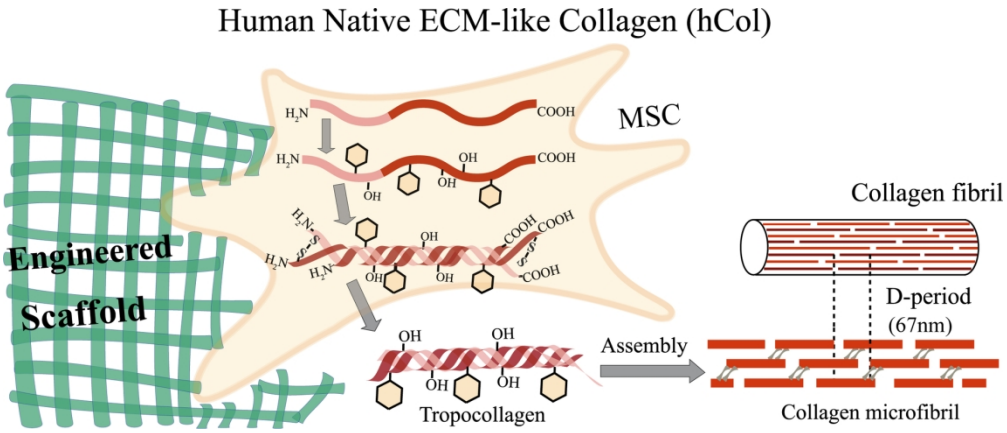

83x35mm (600 x 600 DPI)